

Enhancing Lifelong Multi-Agent Path-finding by Using Artificial Potential Fields

Arseniy Pertzovsky, Roni Stern, Ariel Felner and Roie Zivan

Ben-Gurion University of the Negev

Abstract. We explore the use of Artificial Potential Fields (APFs) to solve Multi-Agent Path Finding (MAPF) and Lifelong MAPF (LMAPF) problems. In MAPF, a team of agents must move to their goal locations without collisions, whereas in LMAPF, new goals are generated upon arrival. We propose methods for incorporating APFs in a range of MAPF algorithms, including Prioritized Planning, MAPF-LNS2, and Priority Inheritance with Backtracking (PIBT). Experimental results show that using APF is not beneficial for MAPF but yields up to a 7-fold increase in overall system throughput for LMAPF.

1 Introduction

Artificial Potential Fields (APFs) [18] can be used to improve the deployment of mobile agents in an environment with obstacles. When using this physics-inspired approach, each agent is considered a particle that is moved on the basis of the attraction and repulsion forces that are applied to it. Typically, obstacles and other agents generate repulsive forces, while targets and destination goals apply attractive forces [19]. APFs have been used to solve many motion planning problems [29, 14, 8], with successful applications in obstacle avoidance of an unmanned aircraft [35], collision avoidance systems for automated vehicles [53] and more [29].

Multi-agent Pathfinding (MAPF) is the problem of finding paths for a group of agents such that they reach their goals without colliding with each other [45]. Instances of MAPF exist in robotics [3], automated warehouses [55, 36], digital entertainment [27] and more [31]. Solving MAPF is computationally difficult since the number of possible actions at every time point is exponential in the number of agents. In fact, for common optimization criteria, finding an optimal solution for MAPF is NP-hard [56, 46]. Popular optimal and suboptimal algorithms, such as Prioritized Planning (PrP) [41], Conflict-Based Search (CBS) [39], and Large Neighborhood Search for MAPF (MAPF-LNS) [22], mitigate this combinatorial challenge by planning a path for each agent individually and imposing different forms of constraints to avoid collisions. Alternatively, algorithms such as PIBT, LaCAM, and LaCAM* [33, 32, 32], directly search the space of *configurations*, where a configuration is a set of all agents' locations in a given time step.

However, using existing algorithms often results in congestion occurring in areas of the environment that are shared by the shortest paths of multiple agents. This congestion problem is exacerbated when solving *lifelong MAPF* (LMAPF) [22, 48], where an agent receives a new goal location whenever it reaches its current goal location. In LMAPF, congested areas tend to become more and more

congested over time, resulting in a decrease in overall system efficiency. The use of APFs is a natural approach to encourage agents to avoid congested areas, adding repulsion forces not only to avoid obstacles but also to avoid the paths of other agents. In this paper, we explore the potential of this approach.

We first investigate using APFs to solve MAPF problems by following a simple, myopic approach: each agent plans its next move based on the forces of APFs of the other agents. The resulting MAPF algorithm (Direct APF) compares poorly with existing MAPF algorithms on standard MAPF benchmarks. Apparently, relying only on attraction and repulsion forces in MAPF is too myopic, and longer-horizon path planning is needed. We, therefore, explore the addition of APFs into existing MAPF solvers. We integrate APFs into *Temporal A** (TA*) [41] and *Safe Interval Path Planning with Soft constraints* (SIPPS) [24], which are single-agent pathfinding algorithms that plan for individual agents under different types of constraints. We modify the cost of agents' actions to consider the APFs created by other agents who have already planned their paths. Consequently, the path returned for an agent not only optimizes fast arrival at the goal but also avoids areas congested by other agents. We also integrate APFs in a similar way in PIBT, LaCAM, and LaCAM*. Experimental results on a range of standard MAPF benchmark problems show that our APF-augmented algorithms are not effective for classical MAPF. However, they are very effective when solving LMAPF, yielding up to a 7-fold increase in throughput.

2 Definition and Background

A classic MAPF problem is defined by a tuple $\langle k, G, s, g \rangle$ where k is the number of agents, $G = (V, E)$ is an undirected graph, $s : [1, \dots, k] \rightarrow V$ maps an agent to a start vertex, and $g : [1, \dots, k] \rightarrow V$ maps an agent to a goal vertex. Time is discretized into time-steps. In every time-step, each agent occupies a single vertex and performs a single *action*. There are two types of actions: *wait* and *move*. The result of a *wait* action of an agent located in some vertex v at some time-step is that the agent will stay at the same vertex v at the next time-step. The result of a *move* action is that the agent moves to an adjacent vertex v' on the graph (i.e., $(v, v') \in E$). A *single-agent path* for agent a_i , denoted π_i , is a sequence of actions that start from s_i and end in g_i . A solution to a MAPF is a set of single agent paths $\pi = \{\pi_1, \dots, \pi_k\}$, one per agent, that do not *conflict*. Two single-agent paths have a *vertex conflict* if they aim to occupy the same vertex at the same time and a *swapping conflict* if they aim to traverse the same edge at the same time from opposing directions. The *sum-of-costs* (SOC) of a MAPF solution π is the sum over the lengths of

its constituent single-agent paths. It is often desirable to find minimal SOC solutions.

Some MAPF algorithms are *complete and SOC-optimal*, i.e., guaranteed to return a valid optimal SOC solution if such exists. Primary examples of such algorithms are CBS [39], ICTS [38], A*+OD+ID [44], M* [52], BCP [20], and SAT-MDD [47]. Other MAPF algorithms are complete but suboptimal. They are guaranteed to find a solution if such exists, but the cost of the returned solution may not be optimal. Examples of such algorithms are Push-and-Swap [26] and Kornhauser’s algorithm [9].

Prioritized Planning (PrP) and LNS2 PrP [4] is a simple yet very popular MAPF algorithm [21, 51, 58, 6]. In PrP, the agents plan sequentially according to some predefined order. When the i^{th} agent plans, it must avoid the paths chosen for all $i - 1$ agents that have planned before it. PrP is agnostic to how a single-agent path is found for each agent as long as no conflicts with existing plans are generated. Such single-agent paths are found by a low-level search algorithm such as Temporal A* (TA*) or SIPPS, which are described below. PrP is simple and fast but might not be very effective in very dense environments due to possible deadlocks. Large Neighborhood Search for MAPF (LNS2) [24] is an incomplete MAPF algorithm that aims to overcome some of the pitfalls of PrP. LNS2 starts by assigning paths to the agents even if they conflict. LNS2 then applies a *repair* procedure, where PrP is used to replan for a subset of agents, aiming to minimize conflicts with other agents. LNS2 repeats this repair procedure until the resulting solution is conflict-free.

Temporal A*, SIPP, and SIPPS Temporal A*, SIPP, and SIPPS are algorithms that plan a path for a single agent under constraints. They are used in many MAPF algorithms, such as CBS [39], PBS [28], PrP, and LNS2. Temporal A* (TA*) uses A* on the *spatio-temporal state-space* in which a state is a vertex-time pair (v, t) . TA* receives the start and goal locations of an agent, along with a list of vertex- and edge constraints. A vertex constraint is a pair (v, t) specifying that the agent must not plan to be at v at time-step t . An edge constraint (e, t) specifies that the agent must not traverse edge e at time t in either direction. TA* returns the shortest path that avoids the given constraints.

Safe Interval Path-planning (SIPP) [34] improves TA* by dividing time into intervals instead of time-steps to represent the time dimension. SIPP performs an A* search on a state space where each state is defined by a vertex and a safe (time) interval, representing that the agent occupies that vertex in this time interval and that this does not violate any given constraint. Safe Interval Path-planning with Soft Constraints (SIPPS) [24] generalizes SIPP to accept both *hard* and *soft* constraints. SIPPS returns a path that does not violate any hard constraints and minimizes the number of soft constraints violated. SIPPS is designed to run within LNS2. A node n in the SIPPS search tree consists of four elements: a vertex $n.v$; a safe interval $[t_{start}^n, t_{end}^n)$, where t_{start}^n is also called the earliest arrival time; an index $n.id$; and a boolean flag $n.is_goal$ indicating whether the node is a goal node. The f -value of node n is the sum of its g -value and h -value, where the g -value is set to t_{start}^n and the h -value is a lower bound on the minimum travel time from vertex $n.v$ to vertex g . Each node n also maintains a c -value, which is the (underestimated) number of soft collisions in the partial path from the root node to node n . SIPPS first prioritizes nodes according to smaller $c(n)$ values. In case of a tie, it moves to the secondary priority and prefers nodes with smaller $f(n) = g(n) + h(n)$.

PIBT and LaCAM PIBT [33] is a MAPF algorithm that searches in the *configuration space*. A configuration here is a vector repre-

senting the agents’ locations at some time-step. PIBT searches in this space in a greedy and myopic manner, starting from the initial configuration of the agents and iteratively generating a configuration for the next time-step until reaching a configuration where all agents are at their goals. PIBT generates configurations recursively, moving every agent toward its goal while avoiding conflicts with previously planned agents. To avoid deadlocks, PIBT employs priority inheritance and backtracking techniques. PIBT is very efficient computationally but is incomplete since it searches greedily in the configuration space. LaCAM [32] also searches the configuration space in a similar manner. To ensure completeness, LaCAM adds constraints to the configuration generation process to ensure that it can eventually reach every possible configuration. LaCAM* [32] builds on LaCAM but improves its configuration generation process. LaCAM* may also continue the search in an anytime fashion, and it eventually converges to the optimal solution.

2.1 Lifelong MAPF (LMAPF)

Lifelong MAPF (LMAPF) [22] is a version of *online MAPF* [48] where agents continuously receive new tasks from a task assigner (outside the path-planning system). When an agent reaches its current goal, it receives a new goal to travel to from the task assigned. The task in classical MAPF is to minimize the cost of the solution. Since solving LMAPF involves solving multiple MAPF problems, the efficiency of LMAPF algorithms is commonly measured by the overall system *throughput* achieved, which is measured by the number of tasks completed in a given period of time [23, 30].

The Rolling-Horizon Collision Resolution framework (RHCR) [23], solves MAPF problems by repeatedly planning the next k steps (k is the *horizon* parameter) to execute based on the current locations and goals of the agents. The agents then move $w \leq k$ steps, where w is a *window* parameter, and the process repeats. RHCR is particularly useful in LMAPF as new goals are generated on the fly and there is no point in planning long paths.

Congestion avoidance techniques Several approaches were proposed to avoid the emergence of congested areas in LMAPF. Han et al. [16] used database heuristics that are customized for every map separately. They also proposed a Space Utilization Optimization heuristic for clever tie-breaking that still preserves optimality [17]. Surynek et al. [42] developed a reinforcement learning (RL) approach for a partially observable variant of MAPF. In our work, we neither restrict observability nor do we require a pre-processing stage for training. Therefore, we do not compare our work with these approaches. Chen et al. [7] proposed to exploit time-independent routes to compose a heuristic for the PIBT algorithm that predicts future expected congestion. Our method for incorporating APFs in PIBT is inspired by their work.

2.2 Artificial Potential Fields

APFs are commonly used for single-agent motion planning in continuous spaces [2, 13, 54, 8, 29, 57, 40]. Vadakkepat et al. [49] studied continuous spaces with moving obstacles. Hagebäck et al. [15, 14] used APFs in real-time strategy games to avoid obstacles. Other works dealt with multiple agents. Liu et al. [25] used APFs in a problem of formation control; Dinh et al. [11] introduced Delegate MAS that simulated food foraging behavior in ant colonies; and many works [37, 12, 1, 10] introduced reinforcement learning algorithms (RL) that incorporated APFs together with Optimal Reciprocal Collision Avoidance (ORCA) [50] or Force-based motion

planning (FMP) [37]. Some algorithms include APFs as part of the environment [5]. To the best of our knowledge, we are the first to apply APFs to solve MAPF problems.

3 Direct Artificial Potential Fields

In this section, we present a *direct application* of APFs (DAPF) to solve MAPF problems. In DAPF, at every time-step each agent a_i sums a set of repulsion and attraction “forces” and moves in the corresponding direction. These “forces” consist of repulsion from the locations of all other agents and attraction to the location of the goal of a_i . We experimented with different functions for these repulsion and attraction “forces” in our MAPF context. The following functions worked reasonably well in our experiments.

Repulsion forces: for every agent a_i , we create a repulsion function APF_i based on its current location v_i .

$$APF_i(v) = \begin{cases} 0 & \text{if } d(v_i, v) > d_{max} \\ w \cdot \gamma^{-d(v_i, v)} & \text{otherwise} \end{cases} \quad (1)$$

where d_{max} , γ , and w are predefined parameters and $d(v_i, v)$ is the minimal distance between v and v_i .¹ The w parameter controls the strength of the repulsion, γ controls the rate of decay, i.e., how fast its intensity of the repulsion decreases while moving away from its source, and d_{max} defines how far away from v_i the repulsion affects the cost.²

Attraction forces For every agent a_i , we create an attraction function $GoalAPF_i$, based on its goal g_i :

$$GoalAPF_i(v) = \begin{cases} h(g_i, v) & \text{for agent } a_i \\ 0 & \text{for other agents} \end{cases} \quad (2)$$

where $h(g_i, v)$ is a precalculated heuristic estimation on the distance from vertex v to g_i . Given these repulsion and attraction functions, DAPF moves in every time-step each agent a_i located at v_i to the adjacent location v'_i that minimizes

$$Total_APF(v'_i) = \sum_{j \neq i} APF_j(v'_i) + \sum_j GoalAPF_i(v'_i) \quad (3)$$

Ties are broken randomly. Collisions are avoided in a prioritized planning manner. The agents plan sequentially (with some random order), where every agent cannot occupy the current locations of other agents and the locations reserved by previously planned agents.

DAPF is very efficient computationally. In every iteration, each agent incurs a runtime of $O(k \cdot (d_{max})^2)$, where k is the number of agents and d_{max} is the radius of influence of APFs. So, the overall runtime complexity of DAPF is $O(k^2 \cdot (d_{max})^2 \cdot N)$, where N is the number of iterations.

In spaces with relatively few obstacles and a small number of agents, using DAPF is very fast. However, it performed poorly in our experiments when the environment became more dense. This is because there are cases where long-term planning is needed and a naïve usage of APFs, as done by DAPF, is insufficient no matter which parameters we choose. For example, consider the MAPF problem in Figure 1 (a). Solid lines point to the agents’ goal locations. Here, DAPF fails to find a solution. Agents are pushed into and pulled

¹ This could be the exact minimal distance in the graph or some estimation heuristic on it. In our experiments, every agent location is associated with a cell in a grid. We used Manhattan distance.

² We illustrate this in the supplementary material.

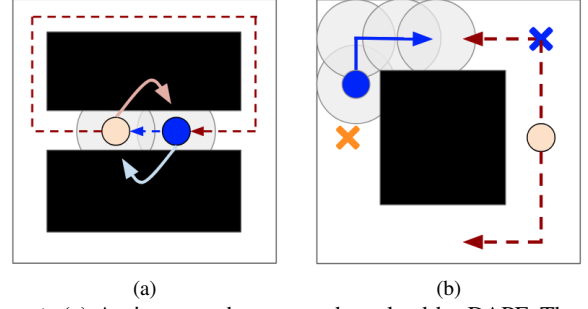


Figure 1: (a) An instance that cannot be solved by DAPF. The dotted lines depict a PrP solution. (b) Two agents solve LMAPF. The X shapes represent goal locations. A solid blue line shows the direction of a chosen path for the blue agent. Dashed red lines represent alternative k -length paths for the orange agent. The agent will prefer the bottom path because of the APFs of the path of the blue agent back to the middle corridor, preventing agents from swapping positions. The possible solution is for the orange agent to bypass the obstacle and reach its goal (dashed line in Figure 1 (a)). In the following sections, we propose a range of techniques for using APFs within existing MAPF algorithms.

4 Integrating APFs in TA* and SIPPS

Many MAPF algorithms internally use either TA* or SIPPS to find paths for individual agents. We propose to use APFs within these single-agent path-finding algorithms such that the resulting path not only avoids collisions with the paths of other agents but also attempts to keep distance from them by taking into consideration the repulsion of their APFs. We refer to our TA* and SIPPS variants as *Temporal A* with APFs* (TA*+APF) and *SIPPS with APFs* (SIPPS+APF), respectively.

4.1 Temporal A* with APFs

TA*+APF is a single-agent path-finding algorithm. It accepts as input a tuple $\langle G(V, E), s, g, \{\pi_1, \dots, \pi_{k'}\} \rangle$ where G is the graph of possible locations the agent can occupy (V) and the allowed transitions between them (E); s and g are the start and goal locations of the path planning agent; and π_i is a path for agent a_i for every $i = 1, \dots, k'$. The output of TA*+APF is a path from s to g that does not conflict with any of the paths $\pi_1, \dots, \pi_{k'}$. The given set of paths $\{\pi_1, \dots, \pi_{k'}\}$ depend on the particular MAPF algorithm in use. For example, in PrP TA*+APF will be given the paths planned for the higher-priority agents. In LNS2, the given set of paths includes the paths already planned for the other agents within the neighborhood of the planning agent.

To bias the resulting path to keep distance from these paths, TA*+APF creates for every path $\pi_i \in \{\pi_1, \dots, \pi_{k'}\}$ a repulsion APF function APF_i that maps every location-time pair (v, t) to a real number representing the added penalty incurred by planning to occupy v at time t . TA*+APF considers these penalties when computing the cost of every move. There are multiple ways to define these repulsion APF functions and aggregate them into a single penalty cost. We experimented with several options and have found the following implementation to work best in our experimental setup. Similar to DAPF, the APF induced by agent a_i on location v and time t is computed as follows:

$$APF_i(v, t) = \begin{cases} 0 & \text{if } d(v, \pi_i[t]) \geq d_{max} \\ w \cdot \gamma^{-d(v, \pi_i[t])} & \text{otherwise} \end{cases} \quad (4)$$

where d_{max} , γ , and w are predefined parameters and $d(v, t, \pi_i[t])$ is the minimal distance between v and $\pi_i[t]$.³ The purpose of each parameter is as described in Section 3. The only difference between this computation method compared to the one used by DAPF (Eq. 12) is the introduction of the time dimension. Hence, in each time-step t' an agent considers only APFs that are calculated at t' . In the special case of $d_{max} = 0$, $APF_i(v, t)$ is always 0. This corresponds to plain TA*, which only considers conflicts where agents are exactly at the same location (distance 0 from each other). To aggregate all the APFs we used a simple sum. That is, the APF cost of moving into location v at time is

$$cost_{APF}(v, t) = \sum_{i \in \{1, \dots, k'\}} APF_i(v, t) \quad (5)$$

We considered incorporating our APF-inspired cost function within TA* in two places: as part of the heuristic evaluation function or as part of the edge cost function. For a node n generated by TA*, the former adds a penalty to $h(n)$ and the latter adds a penalty to $g(n)$. We initially incorporated our APF-inspired cost function in $h(n)$ and observed poor results. To understand these results, consider what each value (h and g) represents and its objective. $h(n)$ represents an estimate of the cost from n to the goal. It is designed to guide the search towards finding the goal faster. In contrast, $g(n)$ represents the cost of the best path found so far from the start to n . A*, and subsequently TA*, are designed to minimize the edge cost function and correspondingly find the path to the goal with the lowest g -value. Thus, incorporating APFs into heuristic functions does not directly affect what path TA* returns but rather how quickly the search finds it. In contrast, incorporating APFs into the edge cost function (and thus in the g value) directly results in TA* returning paths that optimize for avoiding other agents' paths.

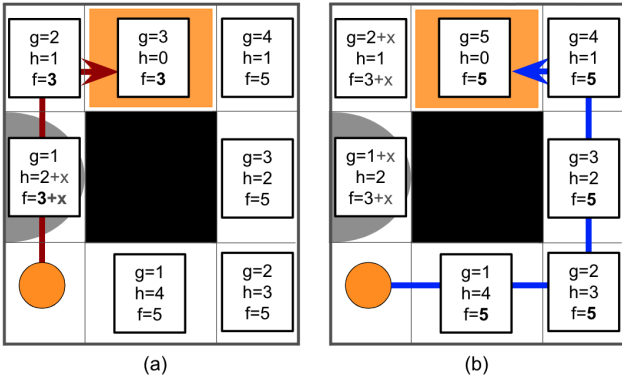


Figure 2: The orange circle and the orange square are the agent's start and goal locations, respectively. x represents the cost of APFs. A* is executed. g , h and f are the components of A* nodes. (a) With $x \leq 2$, an agent always picks a red path wherever x is added. (b) With $x > 2$, the agent picks a blue path if x is added to g . Otherwise, if x is added to h , it continues to choose a red path nonetheless.

Consider Figure 2, where an agent needs to go from the orange circle to the orange square. The components g , h , and f of an A* algorithm are presented inside the locations. The gray zone shows the APFs of another agent that adds the cost x of moving through the location in the middle left of the figure. Consider the case where $x > 2$. A red line is an optimal path that A* would choose if the costs were added to a h component (Fig. 2 (a)). A blue line is an optimal path if the cost is part of a g component, and this is the variant

that we want to implement (Fig. 2 (b)) because we want to avoid the congested gray cell. In other words, h is not being aggregated along paths. It is only defined for individual locations and only attracts the agent towards the goal. In contrast, g is being aggregated and an edge with a large weight will be carried over to all its descendants, and this is what we want.

Therefore, in TA*+APF we add our APF-inspired cost function to the g value of a search node when a node is generated, as follows:

$$g_{APF}(n) = g_{APF}(p) + cost(p, n) + cost_{APF}(v, t) \quad (6)$$

where p is the parent of n , $cost(p, n)$ is the cost of moving the agent from p to n , and (v, t) is the vertex and time-step of node n . TA*+APF runs TA* and prioritizes nodes for expansion according to

$$f(n) = g_{APF}(n) + h(n) \quad (7)$$

Figure 1(b) illustrates an example case, where APFs help to pick a better path out of two options. In this example, two agents work in a RHCR framework. The blue agent plans first and goes directly to its goal. An orange agent has two alternative paths around the obstacle. However, the APFs of the blue agent (gray circles) will cause the orange agent to prefer the bottom path and therefore avoid future conflicts.

Using APFs incurs some computational overhead, compared to vanilla TA*. This overhead is due to the need to compute APFs for every newly generated path. The computational complexity of generating an APF for the path of a single agent is $O((d_{max})^2 \cdot l)$, where $(d_{max})^2$ is the maximal number of nodes affected by the APF induced by an agent occupying a single vertex at a specific time step; and l is the length of the longest path. This computation is done for each of the k agents, adding a total overhead of $O(k \cdot (d_{max})^2 \cdot l)$.

4.2 SIPPS with APFs

SIPPS+APF is based on SIPPS. Thus, a search nodes n in SIPPS+APF represents a vertex $n.v$ and a time interval $[t_{start}^n, t_{end}^n]$, and the input to SIPPS+APF includes a set of *soft constraints* it aims to minimize violating.

We define an APF cost for a SIPPS+APF node n as follows:

$$cost_{APF}(n) = \max_{t \in [t_{start}^n, t_{end}^n]} \sum_{i \in \{1, \dots, k'\}} APF_i(v, t) \quad (8)$$

where $APF_i(v, t)$ is defined in TA*+APF. In other words, $cost_{APF}(n)$ represents the highest APFs an agent can encounter during its time interval.

In SIPPS, the open list is sorted first according to the number of soft collisions violated and then according to $f(n)$. SIPPS+APF follows the same sorting rule, but add the APF costs in each of these components. We explored adding the SIPPS+APF APF costs separately in each of these components, but this yielded limited gains.

In more details, SIPPS+APF maintains for each node n two additional values, $c_{APF}(n)$ and $g_{APF}(n)$, which are computed as follows when n is generated:

$$c_{APF}(n) = c_{APF}(p) + c(p, n) + cost_{APF}(n) \quad (9)$$

$$g_{APF}(n) = t_{start}^n + cost_{APF}(n) \quad (10)$$

where p the parent of n , $c(p, n)$ are the number of soft constraints violated when moving from p to n . SIPPS+APF sorts open list first based on c_{APF} and then based on $g_{APF} + h(n)$.

³ Again, we used Manhattan distance.

The analysis of the runtime complexity overhead incurred by APFs in SIPPS+APF is similar to the analysis described for TA*+APF. An additional computational cost is incurred due to the maximization of the time steps in the relevant safe interval (Eq. 8). So, the overhead equals $O(k \cdot d_{max}^2 \cdot l^2)$, where k , d_{max} , and l are defined as earlier.

4.3 Completeness of TA*+APF and SIPPS+APF

It is important to note that our new idea of using APFs inside the g -value (denoted above as g_{APF}) is only considered when computing the priority of nodes in the open list. However, every node in TA*+APF and in SIPPS+APF still maintains the original spatio-temporal information as in regular TA* and SIPPS. In particular, the original g -value, which adds up the physical steps is still maintained to determine the exact time step for identifying conflicts as well as to prune duplicates. Thus, the search spaces are the same with and without APFs, and the only difference is the order in which nodes are expanded. Consequently, completeness is preserved for both algorithms.

5 PIBT and LaCAM with APFs

Both PIBT [33] and LaCAM [32] use a heuristic to prioritize the actions of agents when generating configurations. In these algorithms, each agent chooses its next action by sorting the vertices adjacent to it based on a heuristic estimate of their distance from the goal. We propose to add APFs to these heuristic estimates and refer to our PIBT variant as *PIBT with APFs* (PIBT+APF). Specifically, when agent i in PIBT+APF picks the next location, it continues to calculate several steps forward, defined by the t_{max} parameter. Those steps follow agent i 's optimal path to its goal and ignore other agents. Then, PIBT+APF builds APFs around these steps with Equation 4 and sums up all the values in the time dimension.

$$PIBT_APF_i(v) = \sum_{j \in \{t_{curr}, \dots, t_{curr} + t_{max}\}} APF_i(v, j) \quad (11)$$

where, t_{curr} defines the current time step. As a result, an APF is created for an agent i . Finally, when every agent sorts the vertices adjacent to its current location, it considers the APFs created by the previously planned agents and sums all the APFs for every neighboring vertex as follows:

$$cost_{APF}(v) = \sum_{i \in \{1, \dots, k' - 1\}} PIBT_APF_i(v) \quad (12)$$

where $PIBT_APF_i(v)$ is defined above (Eq. 11). Finally, we sort the vertices according to $h(v) + cost_{APF}(v)$. The overhead incurred by PIBT-APFs in terms of run-time complexity is $O(k \cdot d_{max}^2 \cdot t_{max})$ per time-step, corresponding to computing $cost_{APF}$ for all k agents and nodes in radius d_{max} . The total overhead is $O(k \cdot d_{max}^2 \cdot t_{max} \cdot l)$, where l is the length of the longest path. Our APF-enhanced version of the LaCAM algorithm uses PIBT+APF for its low-level search. This approach of adapting APFs to PIBT, in part, is inspired by the work of Chen et al. [7] in which the authors use congestion-avoiding paths to navigate agents. Our work can be viewed as the generalization of this approach, where we consider not only the future steps of agents, but also the surrounding locations of these steps. We use their method as a baseline in our experiments.

6 Experimental Study

We conducted an experimental evaluation comparing the use of APFs within PrP [41], LNS2 [24], PIBT [33], LaCAM [32], and LaCAM* [32], where PrP and LNS2 are implemented twice: once with TA* and once with SIPPS as their low-level solver. With APF-enhanced versions, this adds up to a total of 14 algorithms. Versions that use APFs are denoted in our plots by dashed lines. As an additional baseline, we implemented *PIBT with Guide Path* (L-PIBT+GP) from Chen et al. [7]. All experiments were carried out on four different maps from the MAPF benchmark [45]: *empty-32-32*, *random-32-32-10*, *random-32-32-20* and *room-32-32-4*, as they present different levels of difficulty. The number of agents used in our experiments ranged from 50 to 450. We executed 15 random instances per every number of agents, map, and algorithm. The APF parameters used were $w = 1$, $d_{max} = 4$, and $\gamma = 2$ for TA*+APF, $w = 0.1$, $d_{max} = 3$, and $\gamma = 3$ for SIPPS+APF, and $w = 0.1$, $d_{max} = 2$, $\gamma = 3$, and $t_{max} = 2$ for PIBT+APF, which were observed to work best in general across all grids.⁴ All algorithms were implemented in Python and ran on a MacBook Air with an Apple M1 chip and 8GB of RAM.

Negative Results in Standard MAPF In all our standard MAPF experiments, using APFs in PrP, LNS2, PIBT, and LaCAM, yielded either identical or inferior results. We believe that the reason is as follows. In standard one-shot MAPF, APFs are less important because all we need is a single path for each agent that avoids other agents. Thus, avoiding conflicts (strong constraints) is enough to find a valid solution. Furthermore, for PrP and LNS2, when agent a_i plans, then APFs only exist for agents that have already planned before a_i . Thus, the expected benefit of APFs — avoiding congested areas — did not manifest in performance gains. However, finding plans that avoid congested areas can bring significant gains in the lifelong setting, where agents continuously receive new tasks over time. We demonstrate this in the next set of experiments, which evaluate our APF-augmented algorithms within the RCHR framework in a lifelong MAPF setting.

Lifelong MAPF In this set of experiments, we solved LMAPF problems using the RCHR framework with the parameters *window* and planning *horizon* set to 5. Each algorithm was limited by 10 seconds for the planning phase. In planning-failure events, i.e., when an agent could not find a path within the time limit, we followed Morag et al.'s [30] robust MAPF framework using the *AllAgents + iStay + Persist* configuration. This corresponds to having all agents plan in every planning period (*AllAgents*); failing agents stay in their place (*iStay*); and all agents that do have a path and can follow it without conflicts, do so (*Persist*). This configuration is simple to implement, commonly used in prior work, and yields reasonable results compared to other configurations according to Morag et al. [30]. In the planning phase, our experiment halted after each agent performed 100 steps. The main metric in the LMAPF experiments is the average *throughput* of each algorithm, i.e., the number of times that an agent reaches its goals before the aforementioned 100 time-steps limit is reached, averaged over all agents. Throughput is the common metric for measuring the quality of LMAPF algorithms [23, 43, 30].

Figure 3 plots the average throughput of the different algorithms as a function of the number of agents. Solid lines represent original implementations of algorithms, and dashed lines represent our

⁴ A sensitivity analysis of the impact of these parameters is discussed later and in the supplementary material.

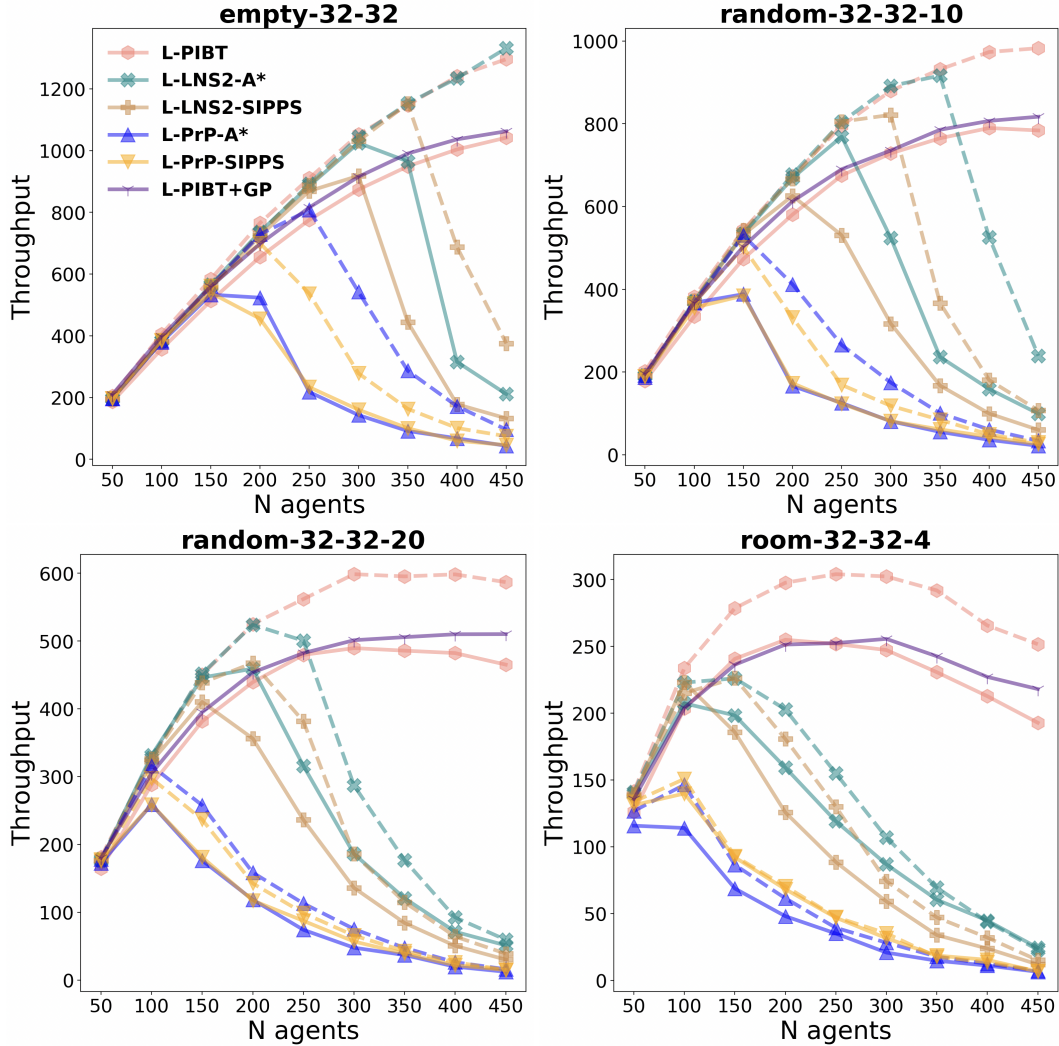


Figure 3: LMAPF: Average Throughput. Dashed lines - APF-enhanced; Solid lines - no APFs

APF-enhanced versions of the same algorithms. The results for LaCAM and LACAM* with and without APFs were virtually the same as for PIBT due to the fact that both LaCAM and LACAM* use PIBT as their low-level search algorithm. Therefore, we only plot the results of PIBT. The results clearly show that using APFs significantly increases the throughput of all other algorithms on all maps. For example, in the *empty-32-32* grid, LNS2 with TA*+APF reaches a throughput of around 1400 with 450 agents, which is approximately 7 times more than the throughput of vanilla LNS2 for the same number of agents. The significant advantage observed in using TA*+APF within the RHCR framework may suggest that it indeed achieves its intended purpose: biasing agents towards paths that avoid the paths of other agents, reducing future collisions and congestion. In most cases, PIBT+APF outperforms other approaches, including L-PIBT+GP, and improves the original PIBT by a significant margin. For example, in the *room-32-32-4* grid, the throughput of PIBT+APF is higher by 20% on average compared to PIBT. As an interesting side phenomenon, we observed the superior performance of LNS2 algorithms using A*, compared to LNS2 with SIPPS. This could be due to the fact that A* prioritizes short paths and SIPPS prioritizes paths with minimum soft constraints.

To summarize, while APFs did not improve performance for standard MAPF they were found to be very helpful in LMAPF for all

algorithms. In LMAPF agents need to continuously plan new paths. Thus, avoiding congested areas is very important and APFs play a significant role in achieving this.

Parameter Sensitivity Analysis Our APF algorithms require setting several parameters, d_{max} , γ , w , and t_{max} . Next, we present a sensitivity analysis for these parameters. As a representative example, we focus on the algorithm that performs the best in our experiments, PIBT+APF. We show the impact of the PIBT+APF parameters, d_{max} , γ , w , and t_{max} on the overall performance in our LMAPF experiments. We only report results on the *room-32-32-4* map, but similar trends were observed with other algorithms and other maps.

Figure 7 plots the average throughput as a function of the number of agents for different values of the parameters. Consider the impact of the w parameter (Fig. 7(a)), which determines how much weight should be given to the cost resulting from APFs as opposed to the regular cost of moving. The impact of the value of this parameter seems to be crucial as different values provide very different results. For example, $w = 0.1$ yielded the best results, while setting $w = 1$ was only slightly better than PIBT (where $w = 0$).

Next, consider the impact of varying d_{max} (Fig. 7(b)). Recall that d_{max} defines how far away from an agent's planned location a potential field reaches. The results show that setting d_{max} to either ex-

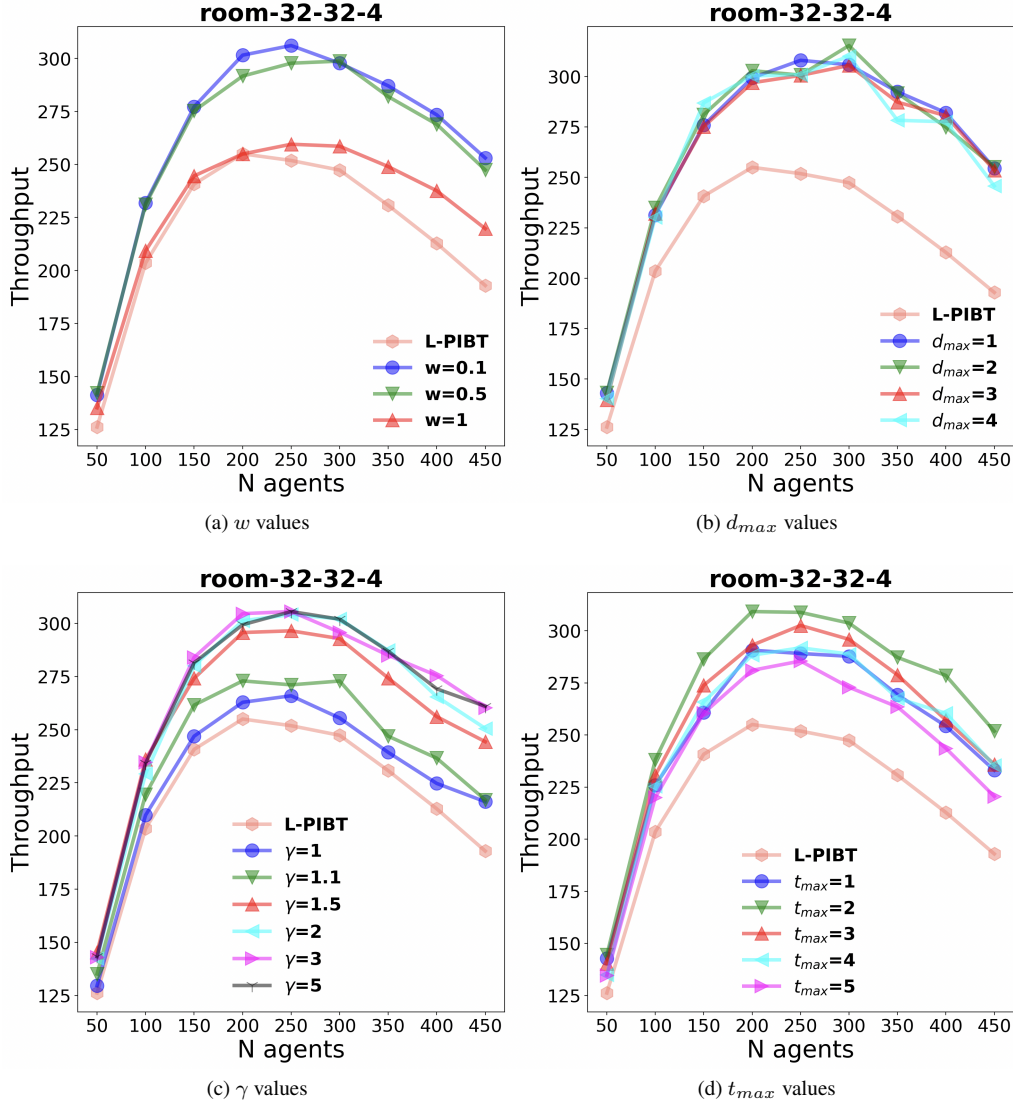


Figure 4: Parameter sensitivity analysis. The “L-PIBT” label designates the original PIBT algorithm that does not utilize APFs.

treme value, too small ($d_{max}=1$) or too high ($d_{max}=4$), yields very similar results. We chose $d_{max}=2$, as it was the one to yield the best performance in all other grids.

Fig. 7(c) analyzes the impact of γ , which defines how fast the impact of the APF decreases with the distance from its origin. Setting $\gamma = 1$ corresponds to an APF that has a uniform effect regardless of distance, as long as the distance is smaller than d_{max} . This assignment of $\gamma = 1$ yielded similar results to vanilla PIBT. All other values of γ yielded much better results, where $\gamma = 2$ worked best in all settings.

Finally, consider the t_{max} (Fig. 7(d)), which defines how many steps forward PIBT+APF builds a future path that ignores other agents and creates APF around the path. Interestingly, $t_{max} = 2$ yielded significantly better results than all other values, neither lower nor greater than 2.

7 Conclusion and Future Work

We investigated whether MAPF can be solved efficiently using artificial potential fields (APFs). First, we showed that a direct implemen-

tation of APFs in a myopic manner is fast but may yield poor results. Then, we proposed to use APFs in TA* and in SIPPS, which are key components of many MAPF algorithms. Specifically, we incorporated APFs in the calculation of the g component of TA*’s node evaluation function and the c and g components of SIPPS’s node evaluation functions. Next, we proposed a way to incorporate APFs into the PIBT and LaCAM algorithms. The resulting algorithms add bias to the search to avoid passing near the paths of other agents.

Experimentally, we showed that the introduction of APFs in other algorithms did not yield any advantage when solving a single offline MAPF problem. However, in the context of lifelong MAPF, we showed that using APFs in TA*, SIPPS, and PIBT is highly beneficial, resulting in significantly higher overall system throughput.

There are several interesting directions for future work. One such direction is to study how to effectively set the parameters d_{max} , γ , t_{max} , and w for APF in TA*, SIPPS and PIBT. Another direction is to examine better ways to incorporate APFs to solve one-shot MAPF problems.

References

- [1] A. Agrawal, S. Hariharan, A. S. Bedi, and D. Manocha. Dc-mrta: Decentralized multi-robot task allocation and navigation in complex environments. In *IROS*, pages 11711–11718. IEEE, 2022.
- [2] J. Barraquand, B. Langlois, and J.-C. Latombe. Numerical potential field techniques for robot path planning. *IEEE Transactions on Systems, Man, and Cybernetics*, 22(2):224–241, 1992.
- [3] R. Barták, J. Švancara, V. Škopková, D. Nohejl, and I. Krasičenko. Multi-agent path finding on real robots. *AI Communications*, 2019.
- [4] M. Bennewitz, W. Burgard, and S. Thrun. Optimizing schedules for prioritized path planning of multi-robot systems. In *ICRA*, volume 1, pages 271–276, 2001.
- [5] M. Bettini, R. Kortvelesy, J. Blumenkamp, and A. Prorok. Vmas: a vectorized multi-agent simulator for collective robot learning. *arXiv preprint arXiv:2207.03530*, 2022.
- [6] S.-H. Chan, R. Stern, A. Felner, and S. Koenig. Greedy priority-based search for suboptimal multi-agent path finding. In *SoCS*, pages 11–19, 2023.
- [7] Z. Chen, D. Harabor, J. Li, and P. J. Stuckey. Traffic flow optimisation for lifelong multi-agent path finding. In *AAAI*, volume 38, pages 20674–20682, 2024.
- [8] R. Daily and D. M. Bevly. Harmonic potential field path planning for high speed vehicles. In *2008 American Control Conference*, pages 4609–4614. IEEE, 2008.
- [9] P. S. Daniel Kornhauser, Gary Miller. Coordinating pebble motion on graphs, the diameter of permutation groups, and applications. In *FOCS*, 1984.
- [10] S. Dergachev and K. Yakovlev. Distributed multi-agent navigation based on reciprocal collision avoidance and locally confined multi-agent path finding. In *CAE*, 2021.
- [11] H. T. Dinh, R. van Lon, and T. Holvoet. Multi-agent route planning using delegate mas. In *Workshop on Distributed and Multi-Agent Planning*, pages 24–32. London, UK, 2016.
- [12] T. Fan, P. Long, W. Liu, and J. Pan. Distributed multi-robot collision avoidance via deep reinforcement learning for navigation in complex scenarios. *IJRR*, 39(7):856–892, 2020.
- [13] D. Fox, W. Burgard, and S. Thrun. The dynamic window approach to collision avoidance. *IEEE Robotics & Automation Magazine*, 4(1): 23–33, 1997.
- [14] J. Hagelback and S. Johansson. A multi-agent potential field-based bot for a full rts game scenario. In *AAAI*, volume 5, pages 28–33, 2009.
- [15] J. Hagelback and S. J. Johansson. Using multi-agent potential fields in real-time strategy games. In *AAMAS*, pages 631–638, 2008.
- [16] S. D. Han and J. Yu. Ddm: Fast near-optimal multi-robot path planning using diversified-path and optimal sub-problem solution database heuristics. *IEEE RA-L*, 5(2):1350–1357, 2020.
- [17] S. D. Han and J. Yu. Optimizing space utilization for more effective multi-robot path planning. In *ICRA*, pages 10709–10715. IEEE, 2022.
- [18] O. Khatib. The potential field approach and operational space formulation in robot control. In *Adaptive and Learning Systems: Theory and Applications*, pages 367–377. Springer, 1986.
- [19] Y. Koren and J. Borenstein. Potential field methods and their inherent limitations for mobile robot navigation. In *ICRA*, pages 1398–1404, 1991.
- [20] E. Lam, P. Le Bodic, D. Harabor, and P. J. Stuckey. Branch-and-cut-and-price for multi-agent path finding. *Computers & Operations Research*, 144:105809, 2022. URL <https://www.sciencedirect.com/science/article/pii/S0305054822000946>.
- [21] C. Leet, J. Li, and S. Koenig. Shard systems: Scalable, robust and persistent multi-agent path finding with performance guarantees. In *AAAI*, pages 9386–9395, 2022.
- [22] J. Li, Z. Chen, D. Harabor, P. Stuckey, and S. Koenig. Anytime multi-agent path finding via large neighborhood search. In *IJCAI*, 2021.
- [23] J. Li, A. Tinka, S. Kiesel, J. W. Durham, T. K. S. Kumar, and S. Koenig. Lifelong multi-agent path finding in large-scale warehouses. *AAAI*, May 2021.
- [24] J. Li, Z. Chen, D. Harabor, P. J. Stuckey, and S. Koenig. Mapf-Ins2: Fast repairing for multi-agent path finding via large neighborhood search. In *AAAI*, 2022.
- [25] X. Liu, S. S. Ge, and C.-H. Goh. Formation potential field for trajectory tracking control of multi-agents in constrained space. *International Journal of Control*, 90(10):2137–2151, 2017.
- [26] R. J. Luna and K. E. Bekris. Push and swap: Fast cooperative path-finding with completeness guarantees. In *IJCAI*, 2011.
- [27] H. Ma, J. Yang, L. Cohen, T. K. S. Kumar, and S. Koenig. Feasibility study: Moving non-homogeneous teams in congested video game environments. In *AIIDE*, 2017.
- [28] H. Ma, D. Harabor, P. J. Stuckey, J. Li, and S. Koenig. Searching with consistent prioritization for multi-agent path finding. In *AAAI*, pages 7643–7650, 2019.
- [29] T. T. Mac, C. Copot, D. T. Tran, and R. De Keyser. Heuristic approaches in robot path planning: A survey. *Robotics and Autonomous Systems*, 86:13–28, 2016.
- [30] J. Morag, R. Stern, and A. Felner. Adapting to planning failures in lifelong multi-agent path finding. In *SoCS*, 2023.
- [31] R. Morris, C. S. Pasareanu, K. S. Luckow, W. Malik, H. Ma, T. S. Kumar, and S. Koenig. Planning, scheduling and monitoring for airport surface operations. In *AAAI Workshop: Planning for Hybrid Systems*, 2016.
- [32] K. Okumura. Lacam: Search-based algorithm for quick multi-agent pathfinding. In *AAAI*, volume 37, pages 11655–11662, 2023.
- [33] K. Okumura, M. Machida, X. Défago, and Y. Tamura. Priority inheritance with backtracking for iterative multi-agent path finding. *AI*, 310: 103752, 2022.
- [34] M. Phillips and M. Likhachev. Sipp: Safe interval path planning for dynamic environments. In *ICRA*, pages 5628–5635. IEEE, 2011.
- [35] H. Rezaee and F. Abdollahi. Adaptive artificial potential field approach for obstacle avoidance of unmanned aircrafts. In *AIM*, pages 1–6. IEEE, 2012.
- [36] O. Salzman and R. Z. Stern. Research challenges and opportunities in multi-agent path finding and multi-agent pickup and delivery problems blue sky ideas track. In *AAMAS*, 2020.
- [37] S. H. Semnani, H. Liu, M. Everett, A. De Ruiter, and J. P. How. Multi-agent motion planning for dense and dynamic environments via deep reinforcement learning. *IEEE RA-L*, 5(2):3221–3226, 2020.
- [38] G. Sharon, R. Stern, M. Goldenberg, and A. Felner. The increasing cost tree search for optimal multi-agent pathfinding. *AI*, 195:470–495, 2013.
- [39] G. Sharon, R. Stern, A. Felner, and N. R. Sturtevant. Conflict-based search for optimal multi-agent pathfinding. *AI*, 2015.
- [40] Y. Shin and E. Kim. Hybrid path planning using positioning risk and artificial potential fields. *Aerospace Science and Technology*, 112, 2021.
- [41] D. Silver. Cooperative pathfinding. In *AIIDE*, 2005.
- [42] A. Skrynnik, A. Andreychuk, M. Nesterova, K. Yakovlev, and A. Panov. Learn to follow: Decentralized lifelong multi-agent pathfinding via planning and learning. In *AAAI*, volume 38, pages 17541–17549, 2024.
- [43] S. Song, K.-I. Na, and W. Yu. Anytime lifelong multi-agent pathfinding in topological maps. *IEEE Access*, 11:20365–20380, 2023.
- [44] T. S. Standley. Finding optimal solutions to cooperative pathfinding problems. In *AAAI*, 2010.
- [45] R. Stern, N. R. Sturtevant, A. Felner, S. Koenig, H. Ma, T. T. Walker, J. Li, D. Atzmon, L. Cohen, T. K. S. Kumar, E. Boyarski, and R. Bartak. Multi-agent pathfinding: Definitions, variants, and benchmarks. In *SoCS*, pages 151–158, 2019.
- [46] P. Surynek. An optimization variant of multi-robot path planning is intractable. In *AAAI*, 2010.
- [47] P. Surynek, A. Felner, R. Stern, and E. Boyarski. Efficient sat approach to multi-agent path finding under the sum of costs objective. In *ECAI*, pages 810–818, 2016.
- [48] J. Švancara, M. Vlk, R. Stern, D. Atzmon, and R. Barták. Online multi-agent pathfinding. In *AAAI*, 2019.
- [49] P. Vadakkepat, K. C. Tan, and W. Ming-Liang. Evolutionary artificial potential fields and their application in real time robot path planning. In *Congress on Evolutionary Computation*, 2000.
- [50] J. Van den Berg, S. J. Guy, M. Lin, and D. Manocha. Reciprocal n-body collision avoidance. In *Robotics Research*, pages 3–19, 2011.
- [51] S. Varambally, J. Li, and S. Koenig. Which mapf model works best for automated warehousing? In *SoCS*, 2022. URL <https://www.autostoresystem.com/>.
- [52] G. Wagner and H. Choset. M*: A complete multirobot path planning algorithm with performance bounds. In *2011 IEEE/RSJ international conference on intelligent robots and systems*, pages 3260–3267. IEEE, 2011.
- [53] N. Wahid, H. Zamzuri, M. A. A. Rahman, S. Kuroda, and P. Raksincharensak. Study on potential field based motion planning and control for automated vehicle collision avoidance systems. In *ICM*, pages 208–213, 2017.
- [54] Y. Wang and G. Chirikjian. A new potential field method for robot path planning. In *ICRA*, volume 2, pages 977–982 vol.2, 2000. doi: 10.1109/ROBOT.2000.844727.
- [55] P. R. Wurman, R. D’Andrea, and M. Mountz. Coordinating hundreds of cooperative, autonomous vehicles in warehouses. *AI magazine*, 29(1): 9–9, 2008.
- [56] J. Yu and S. M. LaValle. Structure and intractability of optimal multi-robot path planning on graphs. In *AAAI*, 2013.
- [57] H.-y. Zhang, W.-m. Lin, and A.-x. Chen. Path planning for the mobile

robot: A review. *Symmetry*, 10(10):450, 2018.

[58] S. Zhang, J. Li, T. Huang, S. Koenig, and B. Dilkina. Learning a priority ordering for prioritized planning in multi-agent path finding. In *SoCS*, 2022. URL www.aaai.org.

A Justification for Parameters

To demonstrate the role of each parameter, consider Figure 5. The x -axis is the distance from the agent (in the middle), the y -axis is the value of APFs, and the height of the red bars represents the specific APFs cost for the locations of the specific distance from the agent. All parameters of APFs are constant, except those we want to stir a bit to see the impact. We stir each parameter separately. We can clearly see that the w parameter controls the strength of the repulsion APF (Fig. 5(a)), γ controls the rate of decay, i.e. how fast its intensity declines while moving away from its source (Fig. 5(b)), and d_{max} defines how far away from v_i the repulsion APF will influence the cost (Fig. 5(c)).

B Supplementary Sensitivity Analysis

In addition to the examination of TA*+APF parameters in the main paper, we present a similar analysis of SIPPS+APF and PIBT+APF parameters. Recall, that as a representative example, we focus on the algorithm with the best performance in our experiments — LNS2 with TA*+APF. Here, we present the results only with *random-32-32-10* grid, however, analogous trends were observed in other algorithms and other grids as well.

B.1 SIPPS+APF

Figure 6 plots an average throughput as a function of the number of agents, for different values of d_{max} (Fig. 6(a)), γ (Fig. 6(b)), and w (Fig. 6(c)). Regarding d_{max} and γ , almost all the values resulted in better throughput, when values $d_{max} = 3$ and $\gamma = 3$ were of the best performance. The trend in w was different. For low values, the results were almost always better than a vanilla version. For high values of w the results were inferior to almost every number of agents, except the dense scenarios, where, for example, $w = 3$ succeeded in reaching the highest throughput. In our experiments, we chose $w = 0.1$.

B.2 TA*+APF

We show the impact of the TA*+APF parameters, d_{max} , γ , and w , on the overall performance in our LMAPF experiments. We only report results on the *random-32-32-10* map but similar trends were observed with other algorithms and other maps.

Figure 7 plots the average throughput as a function of the number of agents, for different values of d_{max} , γ , and w . Consider the impact of varying d_{max} (Fig. 7(a)). Recall that d_{max} defines how far away from an agent’s planned location a potential field reaches. The results show that setting d_{max} to either extreme value, too small ($d_{max}=1$) or too high ($d_{max}=10$), yields significantly worse results than setting d_{max} to 4. Yet, even in these cases, APF-enhanced LNS2 significantly outperformed plain LNS2.

Next, consider γ (Fig. 7(b)), which defines how fast the impact of the APF decreases with the distance from its origin. Setting $\gamma = 1$ corresponds to an APF that has a uniform effect regardless of distance, as long as the distance is smaller than d_{max} . This assignment of $\gamma = 1$ yielded even worse results than vanilla LNS2. All other values of γ yielded much better results, where $\gamma = 2$ worked best in this setting.

Finally, consider the impact of the w parameter (Fig. 7(c)), which determines how much weight should be given to the cost stemming from APFs as opposed to the regular cost of moving. The impact of the value of this parameter is interesting because its preferred value depends on the number of agents in the problem. For example, $w = 2$ yielded the best results for problems with 400 agents, while setting $w = 1$ was best for the other. We also explored setting different w values for different agents according to their traveled path length or future path lengths. These methods did not find any significant improvements, and thus their results are not reported.

C MAPF Experiments

In this section, we present results in a standard MAPF setting. The implementation of APFs without the RHCR [22] framework (i.e. original algorithms) yields inferior results. This can be described by the fact that the first agents do not consider others that come afterward and, therefore cannot take advantage of their APFs to, potentially, escape congestion. Whereas in RHCR, the agents may reconsider several times their paths before arriving at a goal. Hence, we omit the results without RHCR. For the rest of the section, all PrP and LNS2 algorithms are implemented within RHCR, where the window size and horizon depth were set to 5, which we found to be effective in our experimental setup. In this set of experiments, a time limit of one minute was imposed. For the sake of clarity, we do not report on APF-enhanced versions of PIBT, LaCAM, and LaCAM*, as they showed no substantial difference from their baseline versions. As we mentioned in the main paper, we conjecture that this is due to the myopic structure of these algorithms, choosing a single step ahead in every iteration. All experiments were performed on four different maps from the MAPF benchmark [45]: *empty-32-32*, *random-32-32-10*, *random-32-32-20*, and *room-32-32-4*, as they present different levels of difficulty. The maps are visualized in the plots in Figure 8.

Success Rate Figure 9 presents the *success rate* (SR) of algorithms in different grids, where the SR is the ratio of problems that could be solved within the allocated time limit. In many cases, APFs helped to boost the performance, such as for PrP versions. But, in some cases, the results were worse with APFs, than without it, such as in LNS2 versions. Regarding the overall view, LaCAM versions succeeded in solving the majority of the problems outperforming others.

Runtime Figure 10 plots the runtime (y -axis) required to solve a given number of instances (x -axis). This is also known as a “cactus” chart. The trend is similar to SR metric. In most cases, the versions of algorithms that used APFs were able to solve more instances in less time than their counterparts. For example, in *empty-32-32* the APF-version of PrP with A* succeeded in solving almost twice as many instances compared to its vanilla variant. On the other hand, in case of LNS2 in *random-32-32-20*, the results of APF-enhanced versions are the same or even poorer.

RSOC Let RSOC denote the ratio between the sum of costs obtained by an APF-enhanced algorithm and the sum of costs obtained by the version of the same algorithm that does not use APFs. That is, RSOC for PrP is the sum of the costs of PrP with APFs divided by the sum of the costs of vanilla PrP. This is intended to evaluate the potential impact of using APFs on solution cost. RSOC smaller than one means APFs reduced the solution cost. Note that we only compute this ratio for problem instances that were solved by both algorithms. Figure 11 presents the RSOC (y -axis) of all the benchmark algorithms for each number of agents (x -axis) for each of our maps.

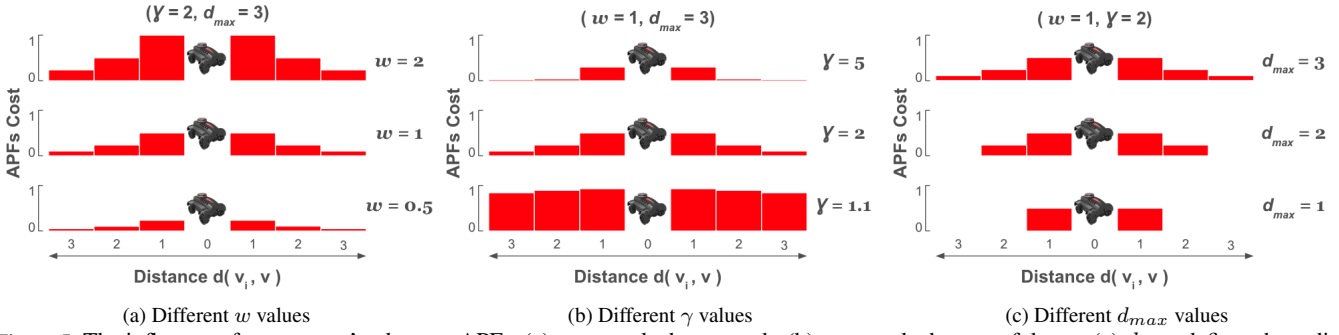


Figure 5: The influence of parameters' values on APFs. (a) w controls the strength; (b) γ controls the rate of decay; (c) d_{max} defines the radius of influence.

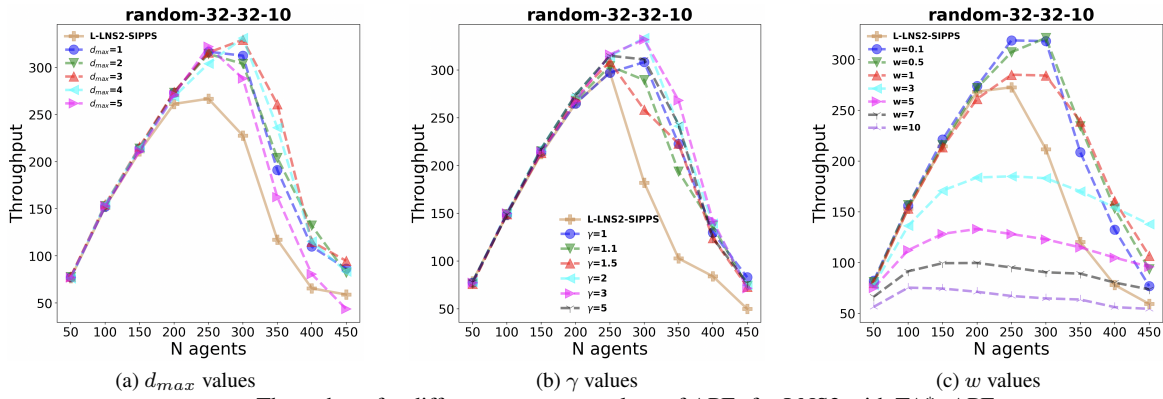


Figure 6: Throughput for different parameter values of APFs for LNS2 with TA*+APF .

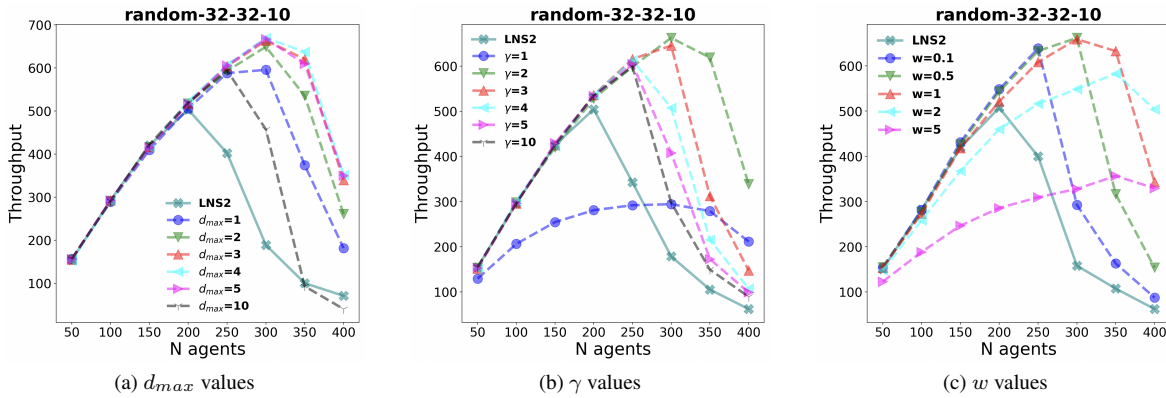


Figure 7: Throughput for different parameter values of APFs for LNS2 with TA*+APF .

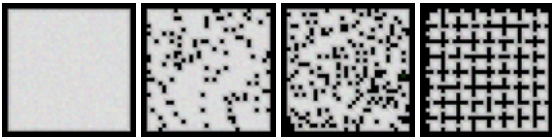


Figure 8: MAPF Grids

We can see that using APFs does not reduce the solution cost compared to vanilla versions. On the contrary, in many cases, it improves the cost. Sometimes, the improvement is two-fold, e.g., PrP versions in *random-32-32-10* grids with 200 agents.

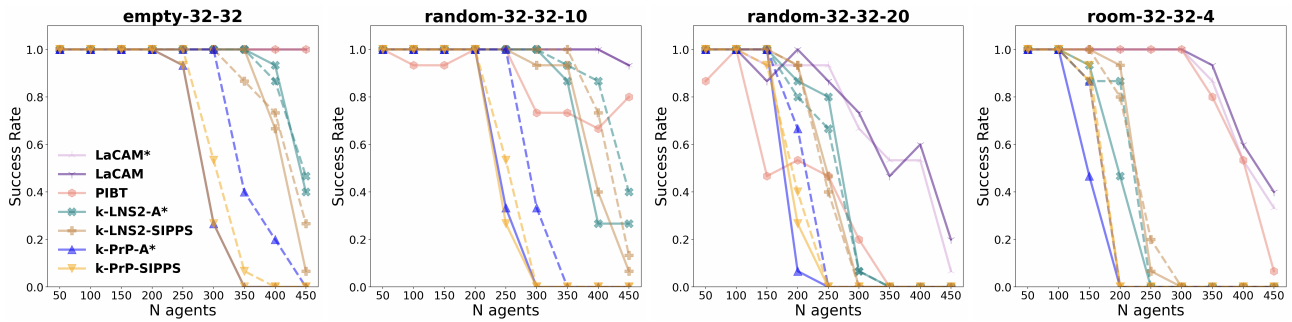


Figure 9: MAPF: Success Rate. Dashed lines - APF-enhanced; Solid lines - no APFs

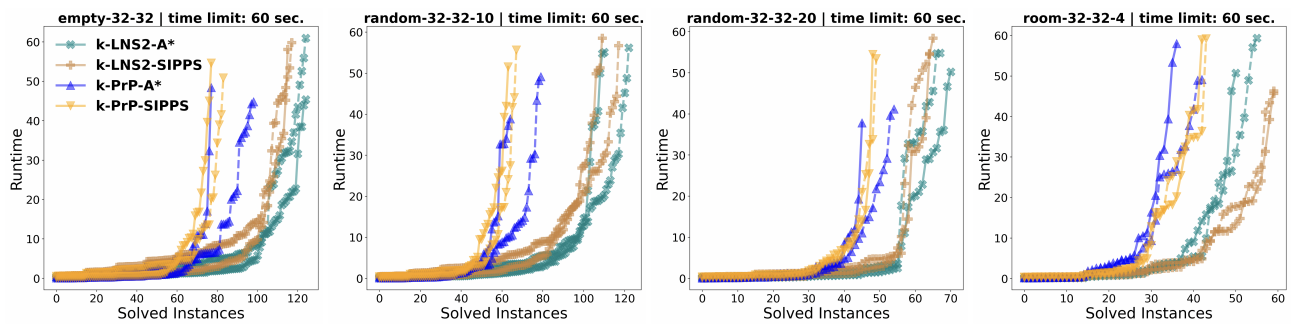


Figure 10: MAPF: Runtime. Plotting the runtime required to solve a given number of instances.

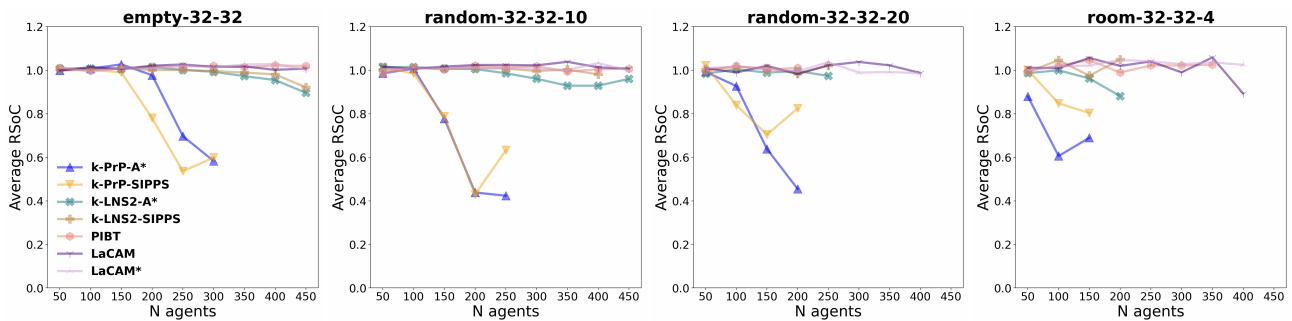


Figure 11: MAPF: RSoC